

UAV-Based Measurement of Sharp Spectral Resonances in Mutually Coupled SKA-Low Elements

Fabio Paonessa^{ID}, Lorenzo Ciorba^{ID}, Georgios Kyriakou^{ID}, Pietro Bolli^{ID}, and Giuseppe Virone^{ID}, *Senior Member, IEEE*

Abstract—Strong mutual coupling between antennas can have detrimental effects in very sensitive radio telescopes based on aperture arrays. For the low-frequency instrument of the square kilometer array, narrowband perturbations in the radiation patterns of the inner elements have been predicted through electromagnetic simulations. This phenomenon deteriorates the spectral smoothness properties and disturbs the station calibration at very specific frequencies. In this letter, we present a new unmanned aerial vehicle (UAV)-based methodology to experimentally characterize such narrowband phenomena with a high-frequency resolution by means of independently-sweeping transmitting and receiving equipment. This solution does not add complexity to the system (e.g., by tethering the UAV). Results and predictions are in good agreement confirming both the presence of spurious resonances and the validity of the simulation approach.

Index Terms—Aperture array, embedded element pattern (EEP), mutual coupling, radio telescope, unmanned aerial vehicle (UAV).

I. INTRODUCTION

In the last two decades, aperture arrays have become an important technology to detect radio astronomical signals with unparalleled performance. For example, the low-frequency instrument of the square kilometer array (SKA-Low)—the most sensitive radio telescope ever conceived—implements an aperture array composed of more than 130 000 log-periodic SKALA4.1 antennas [1] to observe the universe between 50 and 350 MHz.

Each station of SKA-Low is tightly filled with 256 SKALA4.1 antennas producing a relevant mutual coupling phenomenon. Below 100 MHz, the average distance between the closest antennas is lower than $\lambda/2$, meaning that the array works in a dense regime. In this frequency region, there are specific frequencies, namely 55 and 77 MHz, where the mutual coupling significantly perturbs the individual antenna pattern. This has been identified by electromagnetic (EM) simulations using FEKO solver, and its

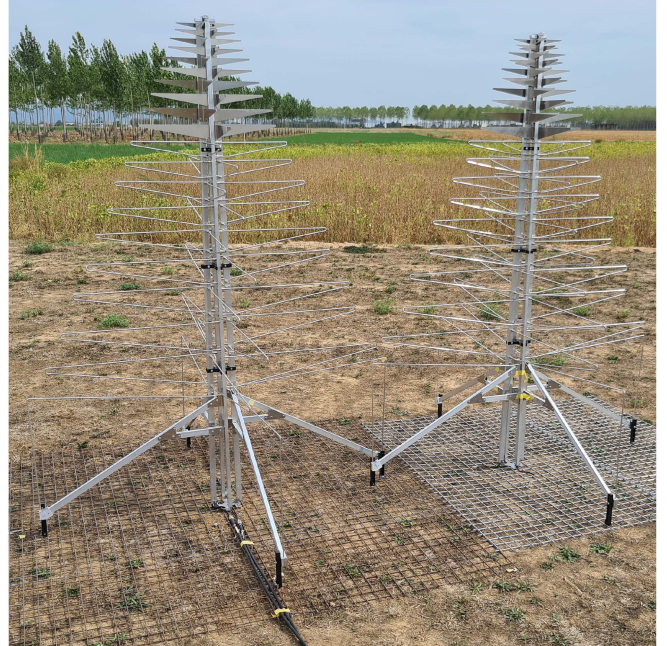


Fig. 1. Two adjacent SKA-Low elements over mesh ground plane. Receiving element on the left-hand side and terminated element on the right-hand side.

spectral degradation was analyzed as a function of the antenna relative positions [2]. The simulation of such resonances of the SKA-Low elements in an array configuration is a very challenging task owing to the complexity of the metal structure (see Fig. 1), the large number of unknowns for the full-station EM mode, and the sharp frequency dependence of the observed coupling phenomenon.

The predicted numerical results, however, have never been checked by measurements at these frequencies. The main novel aspect of this letter is the experimental characterization of such sharp resonances in a relevant environment. We verified the strong mutual coupling between a pair of SKA-Low elements in terms of 1) spectral smoothness of the embedded element gain at zenith and 2) embedded element pattern (EEP) measurements. Such a verification is important for the scientific community as the presence of spurious resonances compromises the overall performance of SKA-Low at specific frequencies. The calibration strategies of the station in fact rely on the smoothness of the EEPs [3].

Manuscript received 15 May 2023; accepted 28 June 2023. Date of publication 30 June 2023; date of current version 1 November 2023. (*Corresponding author:* Fabio Paonessa.)

Fabio Paonessa, Lorenzo Ciorba, and Giuseppe Virone are with the Italian National Research Council (CNR-IEIIT), 10129 Turin, Italy (e-mail: fabio.paonessa@cnr.it; lorenzocior@gmail.com; giuseppe.virone@cnr.it).

Georgios Kyriakou and Pietro Bolli are with the Italian National Institute for Astrophysics (INAF-OAA), 50125 Florence, Italy (e-mail: georgios.kyriakou@inaf.it; pbolli@arcetri.inaf.it).

Digital Object Identifier 10.1109/LAWP.2023.3290967

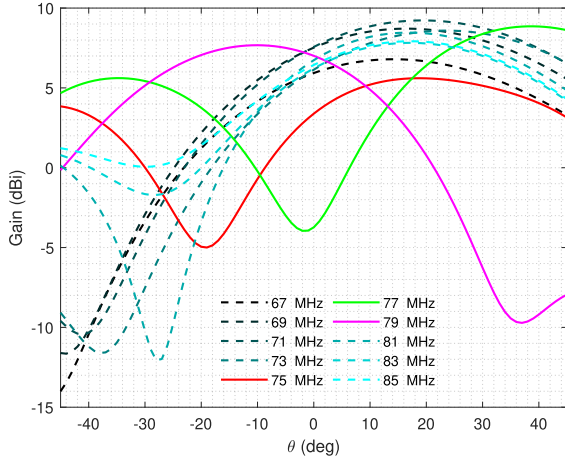


Fig. 2. *E*-plane EEPs, for a set of frequencies, for the EM model of Section II. Negative zenith angles θ are toward the terminated element.

To accomplish the spectral characterization we propose a novel unmanned aerial vehicle (UAV)-based measurement strategy. Differently from previous UAV configurations [4], [5], [6], [7], [8], where the drone radiated either a continuous wave (CW) signal, a comb-like spectrum, or pulses, in this work a stepped swept sine is transmitted and the frequency response of the antenna under test (AUT) is measured without using a synchronous receiver.

The rest of this letter is organized as follows. Section II introduces the SKALA4.1 antenna and the glitch phenomenon. Section III describes the UAV campaign. In Section IV the comparison between numerical and experimental data is presented. Finally, Section V concludes this letter.

II. STRONG COUPLING PHENOMENA BETWEEN ADJACENT SKA-LOW ELEMENTS

The dual-polarized log-periodic SKALA4.1 antenna is formed by 20 dipoles for each polarization, with the longest dipole reaching a length of 1.6 m. For each station of SKA-Low, whose diameter is 38 m, the pseudorandom layout is such that some of the inner elements almost touch each other [2].

Let us define a basic FEKO model composed of two SKALA4.1 antennas laid over an infinite perfect electric conductor, aligned in the *E*-plane and 1.5 m far apart. According to [9], the EEP is the radiation pattern of an excited array element with all other elements terminated. However, since we are operating in receiving mode within the scope of the present work, we refer hereinafter to the polarizations aligned in their *E*-plane as *receiving* and *terminated* element, respectively. The simulation is conducted by exciting the port of the receiving element, while the nonexcited ports are terminated with $50\ \Omega$ loads. Owing to the asymmetry of the geometry, the EEP is generally tilted from the zenith direction, this is evident in Fig. 2 where the *E*-plane EEPs for several frequencies between 67 and 85 MHz are reported. Moreover, while the curves are rather close to each other for most of the reported frequencies (dashed lines), the trend is lost around 77 MHz where highly perturbed patterns appear (solid lines), with also a deep null at zenith at



Fig. 3. UAV-mounted dipole hovering during the measurement.

77 MHz (about -13 dB with respect to the maximum). This picture highlights the sharp nature of the resonance phenomenon. As described in [2], this is a systematic effect, which is not mitigated by the pseudorandom distribution of the antennas. It has also been investigated using the characteristic modes analysis in terms of the electric far-field response [10], and found to correspond to spuriously excited modes that are supported by the combination of receiving and terminated elements. In that analysis, the spurious resonances show modal eigenvalue proximity to those of a single antenna, emphasizing the mutual coupling challenges of wideband log-periodic designs.

III. MEASUREMENT SETUP

An array of two SKALA4.1 antennas 1.5 m apart (center-to-center) was set up as shown in Fig. 1. It consisted of the AUT (i.e., the antenna with the receiving element) mounted over a $2\text{ m} \times 2\text{ m}$ square-grid ground plane, and a second antenna mounted over a $1.65\text{ m} \times 1.68\text{ m}$ square-grid ground plane. Both the grids had a mesh size of 25 mm and were electrically connected with metal ties. The low-noise amplifier (LNA) on top of the antenna was replaced by a passive connection to avoid nonlinearity phenomena induced by radio frequency interference in the outdoor measurement field. The receiving element was connected to a Agilent E4402B spectrum analyzer (SA) through a 60 m long LMR400 cable, whereas the remaining three ports were terminated with matched loads.

The measurements were performed with a quadcopter featuring real-time kinematic positioning, which ensures a centimeter-level accuracy. As far as the RF payload is concerned, the UAV carried a 2 m long dipole fed by a Valon 5015 frequency synthesizer and a balun (see Fig. 3). The synthesizer produced a stepped swept sine within the range of 66–85 MHz in 0.1 MHz steps with a duration of 1.5 s each. The chosen parameters gave 191 frequency points and 5 min of sweep duration. During this lapse, the UAV hovered steady in the sky at 60 m altitude above ground level at the zenith of the AUT.

It is important to point out some system considerations. First, the onboard transmitter and the SA cannot share a common frequency reference unless a wired link to the UAV is used. In other words, since the SA is not tuned to the transmitter, the two devices will sweep independently of each other. Moreover, the absence of a wired link prevents the devices from directly sharing a common sweep trigger signal. For these reasons, the transmitter sweep cannot be acquired within a single sweep of

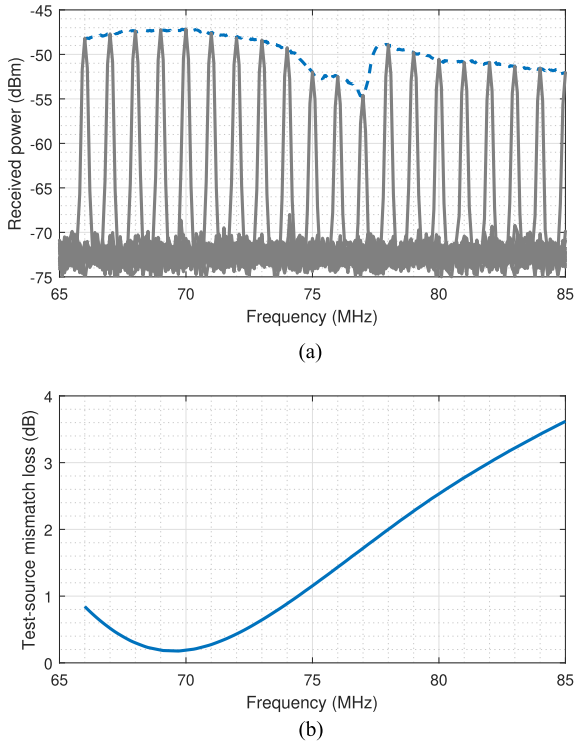


Fig. 4. (a) Twenty out of 191 spectra (solid gray lines) acquired during the sweep measurement, and overall envelope (blue dashed line). (b) Simulated loss due to the mismatch of the UAV-mounted dipole.

the SA. A more convenient approach is to capture, for each frequency point of the transmitter, one SA trace spanning the whole frequency range (66–85 MHz) with short sweep time (e.g., 40 ms). However, if the SA sweep trigger repetition is equal to the transmitter step duration of 1.5 s, there is a small possibility that some SA traces will be systematically acquired at the same time of a frequency change of the synthesizer. To avoid this issue, the SA trigger interval was set to 1 s. This guarantees that even in the worst case that the SA captures the signal during a frequency step, the subsequent acquisition that occurs after 1 s will be successful (the synthesizer is stable for 1.5 s). On the other hand, some frequency points will be acquired twice providing redundancy.

From 300 spectra acquired during the flying time, 191 sweeps containing unique frequencies were selected. The gain response versus frequency was then computed from the envelope of the peaks amplitude [see Fig. 4(a)]. It is worth mentioning that the resonant frequency of the UAV-mounted dipole—i.e., about 70 MHz—falls within the chosen frequency range. However, the loss due to the variable impedance mismatch has been simulated [see Fig. 4(b)] and compensated for.

As far as the AUT is concerned, we verified with full-wave simulations that the limited size of the metal ground plane in the setup of Fig. 1 does not allow a proper characterization of the glitch at 55 MHz. Moreover, the AUT is far better matched at 77 MHz—thus ensuring a good signal-to-noise ratio even in the absence of the LNA—and this frequency is more relevant for scientific research on the epoch of reionization.

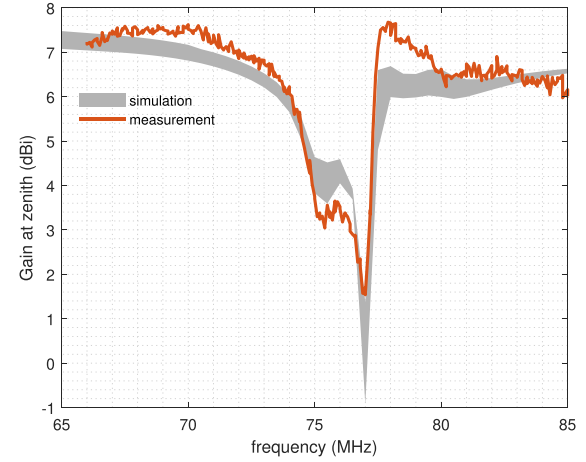


Fig. 5. Measured (orange) curve and simulated (gray envelope) zenith gain versus frequency. A number of five sets of (ϵ_r , σ) were used for the simulations. The measured curve is normalized to the simulated one (baseline model) at 66 MHz.

The physical array configuration did not change for the measurement of the EEPs. In this case, however, the UAV was transmitting a CW signal as it flew along a rectilinear and constant-altitude path lying in the *E*-plane of the EEP with ± 100 m of extension. During the flight, the SA measured the received power at the same center frequency and zero-span mode. The pattern was then computed following the approach of [12] based on the Friis equation.

In the same campaign, we also measured the coupling scattering coefficient S_{21} using the tracking generator output of the SA. This parameter provides an additional validation of the model that does not require the use of the UAV [13]. For this measurement, both receiving and terminated element were connected to the instrument through two separate LMR400 cables, whereas the remaining two polarizations (i.e., those aligned in their *H*-plane) were terminated with matched loads. To remove the effect of the cables, the system calibration was performed via a thru connection at the antenna ports level.

IV. RESULTS

Fig. 5 shows the measured (orange curve) and simulated (gray envelope) zenith gain variation versus frequency. It should be pointed out that the EM model of Section II was refined to reproduce with high fidelity the real setup. In particular, two solid rectangles modeled as perfect electric conductors were placed underneath the antennas and on the top of the surface of a semiinfinite dielectric medium to simulate the soil. This soil volume was included in the solution by means of the Sommerfeld integral equation, which, in FEKO, is hybridized with the method of moments used for the mesh parts (the presence of the soil increases the simulation time by a factor of 4 with respect to a metal-only model). We then varied the soil complex permittivity to account for the margin of error related to its approximate modeling. The gray envelope of Fig. 5 shows the simulated results for five sets of relative permittivity ϵ_r and conductivity σ , and is defined by the min/max of these five models at each frequency.

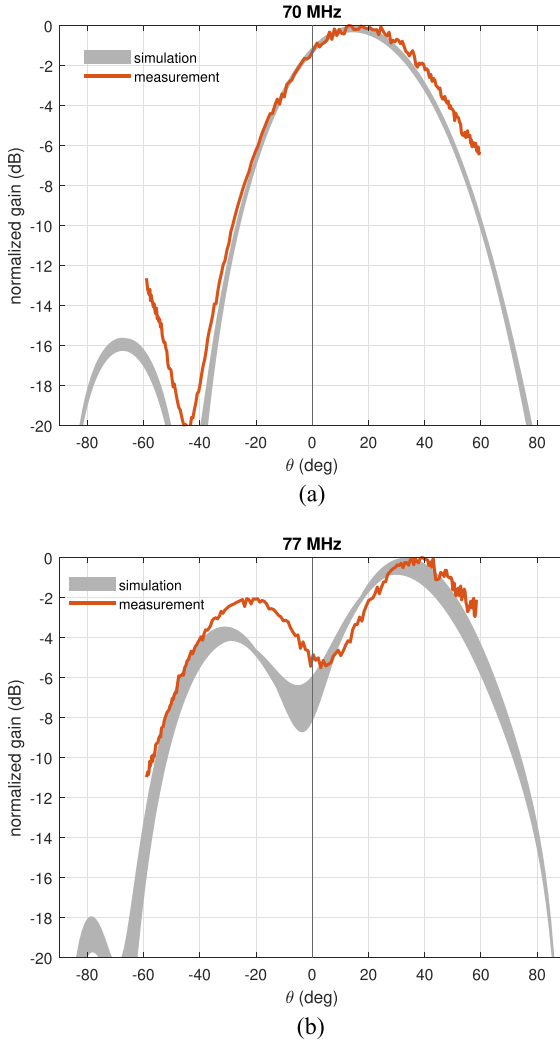


Fig. 6. Measured (orange curve) and simulated (gray envelope) normalized EEPs at (a) 70 and (b) 77 MHz.

For our baseline model, we used a relative dielectric constant of $\epsilon_r = 4$ and a conductivity of $\sigma = 10^{-3}$ S/m, representing mainly dry moisture content of sandy clay loam [11]. To test deviations from these conditions, the more volatile conductivity was scaled by a factor of 5 (i.e., 5×10^{-3} S/m and 2×10^{-4} S/m) while retaining $\epsilon_r = 4$, whereas the dielectric constant was scaled by a factor of 2 (i.e., 2 and 8) while retaining $\sigma = 10^{-3}$ S/m. Within the parameter range, no significant differences occur in the simulated envelope. The agreement between simulations and measurement is remarkable; in particular the simulated gain drop between 75 and 78 MHz is closely followed by the measurement apart from very narrowband and weak noise, with also the small plateaus between 75 and 76 MHz. It should be pointed out that, since the amplitude of the received power is not calibrated, a constant offset has been added to the measurement to align the measured curve to the baseline simulated model at 66 MHz.

In order to ascertain the simulated EEPs, Fig. 6(a) and (b) shows the normalized E -plane EEPs for a minimal set of two frequencies chosen within the unperturbed frequency band (70 MHz) and where the mutual coupling effect is maximum (77 MHz). The simulation envelope corresponding to the extremes of all sets of soil parameters (gray area) covers all the

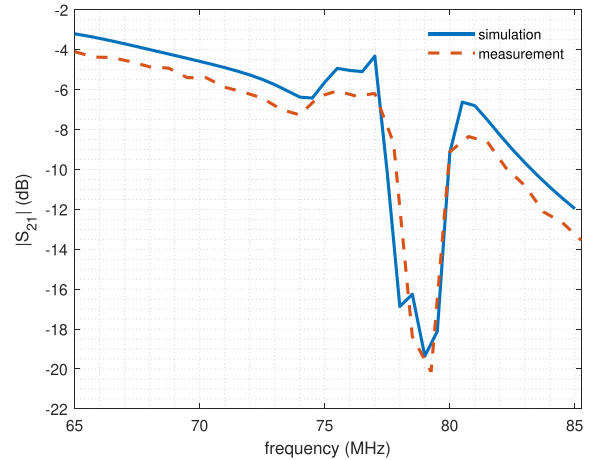


Fig. 7. Measured (orange dashed curve) and simulated (blue curve) $|S_{21}|$ between the adjacent antennas.

zenith angles, whereas the measured curve (orange) is limited to the field of view covered by the UAV flight ($\pm 60^\circ$). While the curves almost perfectly agree in the unperturbed frequency of 70 MHz, an angular offset is present at 77 MHz where the mutual coupling creates a dual lobe. The distribution of radiated power showing a maximum in far-off zenith directions is a nontrivially described phenomenon, as evidenced in [2] and [10], which could lead to small inaccuracies between measurements and simulations. Nevertheless, the perturbed EEP at 77 MHz has been fully confirmed by measurements (similar error levels have been reported in previous publications [8]).

Finally, Fig. 7 shows the $|S_{21}|$ measurement results. The agreement between simulated curve (blue) and the measured curve (dashed orange) is good and within 1 dB for most of the frequencies. Overall, the $|S_{21}|$ trend is a linear decreasing slope likely associated to the larger electrical distance between the two antennas when the frequency increases. On top of that, a remarkable drop in the coupling coefficient is visible between 77 and 80 MHz. It is worth noticing the similarity between the curves across Figs. 5 and 7. These curves, however, refer to different quantities (gain and $|S_{21}|$, respectively), which are not necessarily expected to match. In other words, the two measured quantities show the same resonance phenomenon (at the same receiving port) from two different excitation conditions (i.e., far-field source and adjacent-element port). This explains the small frequency offset observed between the resonance in the two quantities.

V. CONCLUSION

The high density of the inner elements in a SKA-Low station is expected to produce narrowband distortions in the EEPs due to mutual coupling at specific frequencies. On the other hand, the calibration of the digital beamforming system requires accurate knowledge of all the EEPs to reach the expected performance. By exploiting a UAV-based system featuring a frequency-sweeping transmitter, we experimentally verified for the first time such a phenomenon with a high-frequency resolution. The model predictions are confirmed by the experimental results with good agreement.

REFERENCES

- [1] P. Bolli et al., "Test-driven design of an active dual-polarized log-periodic antenna for the square kilometre array," *IEEE Open J. Antennas Propag.*, vol. 1, pp. 253–263, 2020, doi: [10.1109/OJAP.2020.9299109](https://doi.org/10.1109/OJAP.2020.9299109).
- [2] P. Bolli, M. Bercigli, P. Di Ninni, L. Mezzadrelli, and G. Virone, "Impact of mutual coupling between SKALA4.1 antennas to the spectral smoothness response," *J. Astronomical Telescopes, Instrum., Syst.*, vol. 8, no. 1, 2022, Art. no. 011023, doi: [10.1117/1.JATIS.8.1.011023](https://doi.org/10.1117/1.JATIS.8.1.011023).
- [3] S. J. Wijnholds, S. van der Tol, R. Nijboer, and A. J. van der Veen, "Calibration challenges for future radio telescopes," *IEEE Signal Process. Mag.*, vol. 27, no. 1, pp. 30–42, Jan. 2010, doi: [10.1109/MSP.2009.934853](https://doi.org/10.1109/MSP.2009.934853).
- [4] I. Farhat, D. Cutajar, M. Bezzina, and K. Z. Adami, "Drone characterization approach for radio telescopes," in *Proc. Photon. Electromagn. Res. Symp. - Spring*, 2019, pp. 3016–3018, doi: [10.1109/PIERS-Spring46901.2019.9017723](https://doi.org/10.1109/PIERS-Spring46901.2019.9017723).
- [5] L. Ciorba et al., "Large horizontal near-field scanner based on a non-tethered unmanned aerial vehicle," *IEEE Open J. Antennas Propag.*, vol. 3, pp. 568–582, 2022, doi: [10.1109/OJAP.2022.3173741](https://doi.org/10.1109/OJAP.2022.3173741).
- [6] A. Nelles et al., "Calibrating the absolute amplitude scale for air showers measured at LOFAR," *J. Instrum.*, vol. 10, no. 11, Nov. 2015, Art. no. P11005, doi: [10.1088/1748-0221/10/11/P11005](https://doi.org/10.1088/1748-0221/10/11/P11005).
- [7] G. Virone et al., "Measurement of the LOFAR-HBA beam patterns using an unmanned aerial vehicle in the near field," *J. Astronomical Telescopes, Instrum., Syst.*, vol. 8, no. 1, Nov. 2021, Art. no. 011005, doi: [10.1117/1.JATIS.8.1.011005](https://doi.org/10.1117/1.JATIS.8.1.011005).
- [8] F. Paonessa et al., "SKA-Low prototypes deployed in Australia: Synoptic of the UAV-Based experimental results," *URSI Radio Sci. Lett.*, vol. 2, 2020, doi: [10.46620/20-0021](https://doi.org/10.46620/20-0021).
- [9] *IEEE Standard for Definitions of Terms for Antennas*, IEEE Std 145-2013 (Revision of IEEE Std 145-1993), 6 Mar. 2014, doi: [10.1109/IEEESTD.2014.6758443](https://doi.org/10.1109/IEEESTD.2014.6758443).
- [10] G. Kyriakou, P. Bolli, and G. Virone, "Characteristic modes analysis of mutually coupled log-periodic dipole antennas," in *Proc. 17th Eur. Conf. Antennas Propag.*, 2023, pp. 1–4.
- [11] J. D. González-Teruel et al., "Measurement of the broadband complex permittivity of soils in the frequency domain with a low-cost vector network analyzer and an open-ended coaxial probe," *Comput. Electron. Agriculture*, vol. 195, 2022, Art. no. 106847, doi: [10.1016/j.compag.2022.106847](https://doi.org/10.1016/j.compag.2022.106847).
- [12] G. Virone et al., "Antenna pattern measurements with a flying far-field source (hexacopter)," in *Proc. IEEE Conf. Antenna Meas. Appl.*, 2014, pp. 1–2, doi: [10.1109/CAMA.2014.7003370](https://doi.org/10.1109/CAMA.2014.7003370).
- [13] G. Virone et al., "Strong mutual coupling effects on LOFAR: Modeling and in situ validation," *IEEE Trans. Antennas Propag.*, vol. 66, no. 5, pp. 2581–2588, May 2018, doi: [10.1109/TAP.2018.2816651](https://doi.org/10.1109/TAP.2018.2816651).

Open Access provided by 'Consiglio Nazionale delle Ricerche-CARI-CARE-ITALY' within the CRUI CARE Agreement